



NIH Public Access

Author Manuscript

Cell Rep. Author manuscript; available in PMC 2013 November 30.

Published in final edited form as:

Cell Rep. 2013 May 30; 3(5): 1567–1579. doi:10.1016/j.celrep.2013.04.021.

An aberrant transcription factor network essential for Wnt signaling and stem cell maintenance in glioblastoma

Esther Rheinbay^{1,2,3,4,*}, Mario L. Suvà^{1,2,3,*}, Shawn M. Gillespie^{1,2,3}, Hiroaki Wakimoto⁵, Anoop P. Patel⁵, Mohammad Shahid⁶, Ozgur Oksuz², Samuel D. Rabkin⁵, Robert L. Martuza⁵, Miguel N. Rivera^{2,3}, David N. Louis², Simon Kasif^{4,7}, Andrew S. Chi^{1,2,3,8}, and Bradley E. Bernstein^{1,2,3}

¹ Howard Hughes Medical Institute, Chevy Chase, MD 20815, USA

² Department of Pathology and Center for Cancer Research, Massachusetts General Hospital and Harvard Medical School, Boston, MA 02114, USA

³ Broad Institute of Harvard and MIT, Cambridge, MA 02142, USA

⁴ Bioinformatics Program, Boston University, Boston, MA 02215, USA

⁵ Department of Neurosurgery Massachusetts General Hospital and Harvard Medical School, Boston, MA 02114, USA

⁶ Department of Surgery, Massachusetts General Hospital, Boston MA

⁷ Department of Biomedical Engineering, Boston University, Boston, MA 02215, USA

⁸ Divisions of Neuro-Oncology and Hematology/Oncology and Department of Neurology, Massachusetts General Hospital and Harvard Medical School, Boston, MA 02114, USA

Summary

Glioblastoma (GBM) is thought to be driven by a sub-population of cancer stem cells (CSCs) that self-renew and recapitulate tumor heterogeneity, yet remain poorly understood. Here we present a comparative histone modification analysis of GBM CSCs that reveals widespread activation of genes normally held in check by Polycomb repressors. These activated targets include a large set of developmental transcription factors (TFs) whose coordinated activation is unique to the CSCs. We demonstrate that a critical factor in the set, ASCL1, activates Wnt signaling by repressing the negative regulator *DKK1*. We show that ASCL1 is essential for maintenance and *in vivo* tumorigenicity of GBM CSCs. Genomewide binding profiles for ASCL1 and the Wnt effector LEF1 provide mechanistic insight and suggest widespread interactions between the TF module and the signaling pathway. Our findings demonstrate regulatory connections between ASCL1, Wnt signaling and collaborating TFs that are essential for the maintenance and tumorigenicity of GBM CSCs.

© No copyright information found. Please enter manually.

Correspondence and requests for materials should be addressed to B.E.B. (Bernstein.Bradley@mgh.harvard.edu) or A.S.C. (chi.andrew@mgh.harvard.edu)..

* Equal Contributions

Publisher's Disclaimer: This is a PDF file of an unedited manuscript that has been accepted for publication. As a service to our customers we are providing this early version of the manuscript. The manuscript will undergo copyediting, typesetting, and review of the resulting proof before it is published in its final citable form. Please note that during the production process errors may be discovered which could affect the content, and all legal disclaimers that apply to the journal pertain.

Introduction

The importance of epigenetic regulation in cancer initiation and progression is now well recognized (Baylin and Jones, 2011; Pujadas and Feinberg, 2012). Aberrant DNA methylation patterns and recurrent mutations in genes encoding chromatin-modifying enzymes have been documented in a wide range of tumors. Cancer cells maintain distinctive transcriptional programs that reflect their lineage, differentiation stage and cellular environment. These transcriptional programs are driven by transcription factors (TFs) that interact with regulatory sequences, and by proteins that modulate the chromatin state of specific loci. Transcriptional and epigenetic programs can exhibit striking heterogeneity within a tumor and may distinguish cancer stem cells (CSCs) or other sub-populations of clinical significance. However, these malignant programs and their variability remain poorly understood.

Chromatin state maps provide a general and systematic means for gauging the activity and epigenetic state of promoters, genes and other regulatory elements within a particular cell type (Bell et al., 2011; Zhou et al., 2011). These maps are acquired by coupling chromatin immunoprecipitation with deep sequencing (ChIP-Seq), and are typically applied to histone modifications that mark different types of functional sequence elements. Chromatin data can be integrated with TF recognition motifs or binding profiles to gain more specific insight into the regulators and pathways that activate these sequence elements in specific cellular contexts (ENCODE Project Consortium, 2012; Ernst et al., 2011). Although these approaches have been applied to cancer models to a limited extent (Baylin and Jones, 2011), their potential has yet to be explored systematically.

Glioblastoma (GBM) is the most common malignant brain tumor in adults and is associated with poor prognosis despite aggressive treatment. Transcriptional profiling studies have revealed biologically relevant GBM subtypes associated with survival and response to therapy, as well as specific dysregulated cellular pathways (Huse and Holland, 2010). Furthermore, epigenetic regulators, including the Polycomb repressors EZH2 and BMI1, and specific DNA methylation changes have been linked to disease pathology, prognosis and therapeutic responses (Suva et al., 2009; Bruggeman et al., 2007; Lee et al., 2008). Recent work has also shown that epigenetic resetting by induced pluripotent stem cell reprogramming followed by lineage differentiation can override the malignant properties of GBM (Stricker et al., 2013). However, little is known about the control mechanisms that drive these transcriptional programs and their contribution to the malignant phenotype in GBM.

Recent studies have documented sub-populations of GBM cells with tumor-propagating capacity that are believed to constitute the tumor's driving force and to play a major role in tumor recurrence and resistance to therapy (Bao et al., 2006; Chen et al., 2012; Singh et al., 2004). This subpopulation can be prospectively isolated *ex vivo* with specific cell surface markers (Singh et al., 2003; Son et al., 2009) or defined culture conditions (Lee et al., 2006; Lottaz et al., 2010; Wakimoto et al., 2009) and expanded *in vitro* as gliomaspheres. Upon serial xenotransplantation, these cells initiate tumors that closely phenocopy the patient's parental tumor both morphologically and genetically (Galli et al., 2004; Singh et al., 2004; Wakimoto et al., 2009). Because of their unlimited self-renewal capacity and their ability to seed malignant tumors *in vivo* this sub-population satisfies major criteria for cancer stem cells (CSCs) (Valent et al., 2012).

Here we combined chromatin profiling, computational analysis and directed cellular perturbations to characterize transcriptional and epigenetic regulatory programs in GBM CSCs. Comparative analysis of chromatin maps for GBM CSCs, differentiated GBM cells

and non-malignant neural cells reveals a module of developmental TFs that is coordinately activated in the CSCs. Functional analysis suggests that these TFs play essential roles in GBM CSCs. In particular, we show that ASCL1 directly activates Wnt signaling and is essential for GBM CSC maintenance and *in vivo* tumorigenicity. Genome-wide maps for ASCL1 and the Wnt effector LEF1 suggest specific mechanisms and widespread interplay between the TF module and the signaling pathway. Our findings thus provide global and mechanistic insight into the regulatory programs that drive a CSC-like population critical for GBM pathogenesis.

Results

Comparative epigenomic analysis of GBM CSCs and human astrocytes

We focused our study on four GBM CSC lines derived from different human tumors that were defined functionally through their ability to initiate tumors in a xenotransplantation model (Wakimoto et al., 2009; Wakimoto et al., 2011). These lines grow as gliomaspheres (**Figure 1A**; see Experimental Procedures) and express the CSC cell surface markers CD133 and SSEA-1 (**Figure 1B**) and the neural progenitor intermediate filament Nestin (**Figure S1A**). GBM CSCs show differentiation potential towards the neuronal and astrocytic lineages, as shown by MAP-2 and GFAP expression respectively (**Figures S1B**). Orthotopic xenotransplantation of a limited number of GBM CSCs leads to formation of tumors that recapitulate GBM morphology with diffuse infiltration of the brain parenchyma (**Figure 1C**).

We systematically examined the transcriptional and epigenetic landscapes of GBM CSCs by profiling histone H3 lysine 4 trimethylation (H3K4me3; a marker of transcriptional initiation), lysine 36 trimethylation (H3K36me3; transcriptional elongation), and H3 lysine 4 monomethylation (H3K4me1; candidate enhancers) (**Figure 1D; Table S1**) (Zhou et al., 2011). We also mapped H3 lysine 27 trimethylation (H3K27me3), a repressive mark catalyzed by the Polycomb protein EZH2. For comparison, we also profiled normal human astrocytes (NHA) isolated from fetal brain, ES cell-derived neural stem cells (NS; **Figure S1C-F**) (Conti et al., 2005) and previously characterized serum-cultured GBM cell lines derived from the same patient tumors as our GBM CSCs (Wakimoto et al., 2009). These traditional GBM lines grow as adherent monolayers, do not express GBM CSC cell-surface markers and fail to initiate tumors upon orthotopic xenotransplantation in limiting dilution assays (**Figure S1G-J**).

We initially focused our attention on the four GBM CSC lines using the NHA as normal comparators. For each cell type, we classified over 20,000 gene promoters as “active” (only H3K4me3 detected) or “repressed” (H3K27me3 detected, with or without H3K4me3, or neither mark) (**Figure S2A; Table S2**). H3K27me3-marked promoters are maintained in an inactive state by Polycomb complexes, while promoters with neither mark are frequently repressed through DNA hypermethylation (Meissner et al., 2008). We compared assignments between cell types in order to identify genes that are differentially regulated in a majority of the GBM CSC lines relative to NHA. Promoters that are ‘active’ in NHA retain this state in GBM CSCs in a vast majority of cases (n=11586; 94% of NHA H3K4me3 genes) (**Figure 1E**), consistent with many of these being housekeeping genes (Mikkelsen et al., 2007). In contrast, promoters that are ‘repressed’ in NHA frequently change their chromatin state in GBM CSCs in the following manner. Repressed promoters with H3K27me3 and H3K4me3 (‘bivalent’) in NHA predominantly lose H3K27me3 and become activated in GBM CSCs (n=1057; 59% of NHA bivalent promoters) (**Figure 1E**). Repressed promoters with H3K27me3-only in NHA often lose H3K27me3 and switch to the unmarked state in GBM CSCs (n=591; 48% of NHA H3K27me3 genes). Repressed

promoters that are unmarked in NHA tend to retain this state in GBM CSCs (n=5110; 88%) (**Figure 1E**). Notably, an analogous comparison of NS cells to GBM CSCs also revealed frequent switching of loci from bivalent (or H3K27me3-only) in the non-malignant cells to active/H3K4me3 in the CSCs (61%; **Figure S2B**). In contrast, only 33% of genes with bivalent chromatin state in NS cells switched to active/H3K4me3 in the non-malignant NHA (**Figure S2C**). These statistics suggest that genes marked by H3K27me3 in non-malignant contexts frequently lose the Polycomb-associated mark and switch their chromatin state in GBM CSCs.

We next examined how the chromatin state transitions correspond to changes in gene expression. As expected, genes that switch from ‘bivalent’ in NHA to H3K4me3-only in GBM CSC are expressed at significantly higher levels in the malignant cell lines (**Figure S2D**). In contrast, genes that switch from H3K27me3-only in NHA to unmarked in GBM CSCs show little or no change in their expression, suggesting that transcriptional changes are unlikely to underlie this epigenetic switch (**Figure S2E**). We therefore considered the possibility that these loci may become DNA methylated in the CSCs, as would be consistent with prior reports of Polycomb targets becoming hyper-methylated in cancer (Ohm et al., 2007; Schlesinger et al., 2007; Widschwendter et al., 2007). To test this, we profiled DNA methylation in three GBM CSC lines (see Experimental Procedures). We found that loci marked by H3K27me3-only in the NHA become hyper-methylated in the GBM CSCs at a rate that is two-fold higher than bivalent loci (**Figure 1F**). Taken together, these findings suggest that repressive Polycomb complexes are lost from a subset of their target loci in GBM CSCs, with initially bivalent genes undergoing transcriptional activation and H3K27me3-only genes acquiring DNA hyper-methylation.

Widespread TF activation in GBM CSCs

To gain insight into the regulatory consequences of the chromatin state transitions, we examined the identities of genes with ‘active’ chromatin in GBM CSCs, but ‘repressed’ chromatin in NHA. Unbiased functional enrichment analysis (Dennis et al., 2003) revealed a significant over-representation of terms related to development and transcriptional regulation (**Figure 2A; Table S3**). In contrast, we failed to detect significant enrichment for genes that were repressed in GBM CSCs but active in NHA (**Table S3**). We therefore focused our attention on the set of developmental TFs (n=90) that are differentially activated in GBM CSCs (**Table S4**). These include factors previously associated with GBM such as *SOX2* (Gangemi et al., 2009), *OLIG2* (Ligon et al., 2004), *HEY1* (Hulleman et al., 2009) and several *HOX* genes (Murat et al., 2008). However, most of the TFs we detected have not yet been described in this context. Although the CSC lines used in this study were derived from different patients and harbor different genetic aberrations (Wakimoto et al., 2011), a majority of the implicated TFs is active in all four CSC lines (**Figure 2B**). Conventional mRNA microarray profiles confirm that these TFs are expressed at significantly higher levels in the four CSCs than NHA (**Figure 2C**). Consistent with their role as developmental regulators, most of these TFs are marked with bivalent chromatin or H3K27me3 in ES and NS cells, as well as in primary non-malignant brain sections (**Figure S3**) (Zhu et al., 2013). In contrast, we identified few TFs (n=16) that are selectively repressed in the CSCs (**Figure 2D**). This suggests that a common set of TFs loses Polycomb repression and is induced in GBM CSCs.

To better understand their specificities, we also studied the chromatin states of the activated TF genes in representative cell models, including NHA, ES-derived NS cells, the CSCs and serum-grown GBM cell lines. Clustering the TFs on the basis of their promoter H3K27me3 signals distinguished four subsets: (i) “cancer TFs” active in GBM CSCs and traditional GBM cell lines; (ii) “CSC TFs” exclusively active in GBM CSCs; (iii) “stem-cell TFs”

active in CSCs and NS cells; and (iv) NHA-repressed TFs active in all the other cell types (**Figure 2B**).

ASCL1 induces Wnt signaling in GBM CSCs

The distinctive chromatin patterns of the CSC TFs prompted us to further explore their functional significance (**Figure 2B**; **Figure 1G**). We specifically examined whether any of these TFs affect signaling pathways that are essential for GBM CSC proliferation, such as Notch, Hedgehog and Wnt (Clement et al., 2007; Shih and Holland, 2006; Zheng et al., 2010). We ectopically expressed each CSC TF in NHA and measured the expression of canonical target genes for each of these pathways (**Figure 3A**).

We found that ASCL1 (also known as MASH1) induces *AXIN2*, a canonical Wnt target (**Figure 3A**). *ASCL1* mRNA is highly expressed in all four CSC cell lines but not in NHA or NS cells (**Figure 3B**). To confirm the functional connection between ASCL1 and *AXIN2*, we depleted *ASCL1* in GBM CSCs by shRNA-mediated knockdown (**Figure 3C**), whereupon we observed significantly reduced *AXIN2* expression (**Figure 3D**). We also used a Wnt-responsive luciferase reporter system to test whether ASCL1 control of *AXIN2* is associated with a general induction of Wnt signaling and TCF/LEF transcriptional regulation (Firestein et al., 2008; Veeman et al., 2003). Indeed, ASCL1 increased reporter gene expression >10-fold compared to a control vector with mutated TCF/LEF sites (**Figure 3E**). ASCL1-mediated induction of the reporter was dramatically enhanced by co-stimulation with Wnt3a, suggesting a synergistic mode of action with autocrine or paracrine Wnt stimulation. Taken together, these results establish ASCL1 as a regulator of Wnt signaling in GBM CSCs.

To assess the functional role of ASCL1 in CSC maintenance, we performed single-cell sphere-formation assays of GBM CSCs after shRNA-mediated *ASCL1* knock-down (Clement et al., 2007; Galli et al., 2004). Only 2% of *ASCL1*-depleted CSCs retained the capacity to reform gliomaspheres after 14 days compared to nearly 20% of control cells (**Figure 3F and 3G**). In addition, spheres generated by *ASCL1* knock-down cells were significantly smaller ($p<10^{-14}$; **Figure 3H**). Mice orthotopically injected with *ASCL1*-depleted GBM CSCs showed prolonged survival compared to those xenotransplanted with control CSCs ($p<0.01$; **Figure 3I**). Thus, ASCL1 is essential for maintenance and propagation of GBM CSCs.

We next examined *ASCL1* expression in primary GBMs, using published gene expression profiles (Verhaak et al, 2010; Sun et al., 2006). *ASCL1* is expressed at markedly higher levels in tumors relative to normal brain. However, its expression varies significantly between molecular subtypes (Kruskal-Wallis $p<10^{-16}$), with significantly higher levels in proneural tumors (**Figure 3K**). *ASCL1* also correlates with tumor grade, with increasing expression in Grade II and III astrocytomas and Grade IV GBMs of proneural subtype (**Figure 3L**). The functional link between *ASCL1* and *AXIN2* is further supported by significantly correlated expression across the GBM tumors (Pearson's $r=0.52$; $p<10^{-14}$; **Figure 3J**). Furthermore, flow cytometric staining in acutely dissociated human GBM shows that ASCL1 is expressed in a subpopulation of cells with high levels of SOX2, a marker for GBM subpopulations with CSCs properties (**Figure 3M**, **Figure S4**). This result is supported by *in situ* hybridization (ISH) in human GBM samples where *ASCL1* expression is restricted to a subset of SOX2-positive cells (**Figure 3N**).

ASCL1 promotes Wnt signaling directly by repressing DKK1

To identify the direct regulatory targets of ASCL1, we used ChIP-Seq to map ASCL1 in MGG8 CSCs (see **Experimental Procedures**; **Figure S5**). The mapped ASCL1 binding

sites are highly enriched for its cognate sequence motif and include the known target *DLL1* (**Figure S5**). We found that ASCL1 binds to candidate enhancers (marked by H3K4me1) in the vicinity of several genes involved in Wnt regulation, including *FZD5*, *DKK1*, *TCF7* and *TCF7L1* (**Figure 4A**). To test whether these candidates represent direct functional targets, we ectopically expressed ASCL1 in NHA and measured changes in their expression. The effect of ASCL1 on Wnt pathway genes was moderate with the exception of 10-fold downregulation of *DKK1* (**Figure 4B**). This is consistent with a previous report of ASCL1 being a negative regulator of *DKK1* in small cell lung cancer cell lines (Osada et al., 2008). In GBM CSCs, ASCL1 binds to an H3K4me1-marked regulatory element located 5.7 kb upstream of the *DKK1* TSS (**Figure 4C**) which adopts a chromatin configuration characteristic of an inactive or ‘poised’ enhancer. In NHA, which do not express *ASCL1*, this element is also enriched for H3K27ac and thus assumes an ‘active enhancer’ state, consistent with the high expression of *DKK1* in these cells (**Figure 4D**).

To test whether repression of *DKK1* is the primary mechanism by which ASCL1 modulates Wnt signaling, we simultaneously transfected *DKK1* and *ASCL1* into NHA, and measured Wnt activation using the Wnt reporter. As shown in **Figure 4E**, exogenous DKK1 expression completely abrogates the inducing effect of ASCL1. These data support a model in which ASCL1 activates Wnt signaling by repressing a regulatory element upstream of the negative Wnt regulator DKK1. The association is also supported in clinical contexts by a significant anti-correlation in *ASCL1* and *DKK1* expression across primary GBM tumors (Pearson's $r = -0.6$; $p < 10^{-20}$; **Figure 4F**). Given the dependency of GBM CSCs on Wnt signaling (Zhang et al., 2011; Zheng et al., 2010), this regulatory function may explain the critical role of ASCL1 in GBM CSC maintenance.

LEF1 mediates reciprocal interactions between Wnt signaling and CSC TFs

To gain further insight into the Wnt signaling pathway in GBM CSCs, we mapped LEF1, a high-mobility group TF that regulates Wnt targets (see **Experimental Procedures**; **Figure S6**). We identified over 3000 LEF1 binding sites, which are highly enriched for the LEF/TCF motif and include the known Wnt target *CCND1* (Clevers, 2006). The vast majority of these sites (82%) resides outside of promoter regions, consistent with the original identification of LEF1 at an enhancer (Travis et al., 1991). Notably, nearly half of the CSC and stem-cell TF genes are proximal to H3K4me1-marked candidate regulatory elements bound by LEF1 (**Figure 5A**; **Table S5**). To test whether these TFs are downstream of the Wnt pathway, we measured their expression in NHA cells stimulated with *ASCL1* cDNA and Wnt3a protein. We detected significant induction of six TFs, indicating their responsiveness to Wnt signaling (**Figure 5B**). Taken together, these results suggest that cross-talk between a network of activated TFs and Wnt signaling is critical for maintaining GBM CSC regulatory programs (**Figure 5C**).

Discussion

Cancer genome sequencing and complementary mechanistic studies have accelerated our understanding of cancer genetics. However, technical issues and the heterogeneity typical of many tumors have limited comprehension of the epigenetic aberrations that contribute to tumor pathology. Here we combined recently established epigenomic technologies with an *in vitro* CSC model with tumor initiating capacity in order to characterize the epigenetic and transcriptional programs that drive malignant brain tumors. By comparing these GBM CSCs to serum-grown GBM lines and non-malignant neural cell models, we identify a large network of TFs activated in the CSCs in combinations unlikely to occur in normal physiologic contexts. Derepression of this network is associated with loss of H3K27me3 at TF promoters and may reflect ineffective Polycomb repression in the CSCs. We speculate

that diminished epigenetic silencing and promiscuous TF activation might confer a competitive advantage by allowing GBM CSCs to respond to the varied requirements of their malignant state, altered genetic makeup and environment.

Among the CSC TFs, ASCL1 emerged as a potent upstream regulator of the Wnt signaling pathway, which was recently shown to be critical for GBM CSC maintenance (Zhang et al., 2011; Zheng et al., 2010). *ASCL1* over-expression induces Wnt signaling in normal astrocytes, while its knock-down in GBM CSCs markedly reduces activity of the pathway. We show that Wnt activation is mediated through DKK1, a secreted Wnt inhibitor that is directly repressed by ASCL1. We also find evidence that Wnt signaling feeds back upon the CSC TF genes via multiple LEF1 target sites in their vicinity. The clinical relevance of these interactions is supported by increased *ASCL1* expression in primary astrocytomas and GBMs, and a correlation between *ASCL1* and the Wnt target gene *AXIN2* across tumor samples.

In conclusion, we describe an aberrant epigenetic landscape in GBM CSCs and the induction of a non-physiologic TF module that is linked to Wnt signaling and essential for CSC maintenance and tumorigenicity. Our findings thus shed light on the regulatory circuitry of this CSC model and propose specific factors and interacting pathways as candidates for translational study.

Experimental Procedures

Cell Culture

Surgical specimens of GBM tumors were collected at Massachusetts General Hospital with approval by the Institutional Review Board. Mechanically minced tissue was triturated and then cells were grown as gliomaspheres in serum-free neural stem cell medium [Neurobasal medium (Invitrogen) supplemented with 3 mmol/L L-glutamine (Mediatech), 1X B27 supplement (Invitrogen), 0.5X N2 supplement (Invitrogen), 2 ug/mL heparin (Sigma), 20 ng/mL recombinant human EGF (R & D systems), 20 ng/mL recombinant human FGF2 (R & D systems), and 0.5X penicillin G/streptomycin sulfate], as previously described (Wakimoto et al., 2009). Genomic copy number alterations and tumor xenograft histopathology for these CSCs have been described (Wakimoto et al., 2011). From the same tumors, traditional GBM cell lines, grown as adherent monolayer in DMEM 10% FCS were derived as previously described (Wakimoto et al., 2009). GBM CSC differentiation was induced using 5% FCS and withdrawal of growth factors for 7 days on poly-L-ornithine and laminin coated plates (see below for details). Staining was performed for nestin (Santa Cruz, 1: 400), MAP-2 (Chemicon, 1: 150), and GFAP (Sigma, 1: 400).

Human ES-derived neural stem (NS) cells generated from H9 ES cells were obtained from Millipore and grown and passaged in neural stem-cell medium consisting of a 1:1 mix of DMEM/F12:Neurobasal (Invitrogen), 0.5X N2 (Invitrogen), 0.5X B27 (Invitrogen), 1X Glutamax, and 0.1 mM beta-mercaptoethanol, which was supplemented with 20 ng/ul of both EGF and FGF-2 (R&D). NS cells were grown on poly-L-ornithine and laminin coated plates. Poly-L-ornithine/laminin plates were generated as such: A 20 ug/ml solution of poly-L-ornithine (Sigma) in water was added to plates and plates were incubated at 37°C for 1 hour. The poly-L-ornithine solution was then removed, plates were washed three times with PBS, and then 5 ul/ml solution of laminin (Sigma) in PBS was added to plates and plates were incubated at 37°C for at least 3 hours. Cells were passaged using manual dissociation.

For differentiation into astrocytes, when cells were 80-90% confluent, the media was changed to NS medium with 3% FCS and without EGF or FGF-2. After 4 days, cells were fixed for immunofluorescence. For differentiation into neurons, NS cells were grown to 90%

confluence. Then, medium was changed to either NS medium but without N2 and supplemented with 1X B27 or ENStem-A Neuronal Differentiation Medium (Chemicon) supplemented with L-glutamine (2mM). After 2 weeks cells were fixed for immunofluorescence.

For immunofluorescence cells were washed 1X with PBS and then fixed with 4% paraformaldehyde for 30 minutes. Cells were washed 3X with PBS and blocked for 2 hours (5% normal goat serum, 0.3% Triton X-100, PBS). Then primary antibodies in blocking solution were added and cells were incubated overnight at 4°C. The next day, cells were washed twice with PBS and then 2X with blocking solution. Secondary antibody in blocking solution was added and cells were incubated for 2 hours at room temperature. Cells were then washed 3-5 times with PBS, then counterstained with DAPI/1XPBS solution. Primary antibodies include anti-nestin 1:500 (Chemicon Cat SCR060), anti-Sox2 1:200 (Chemicon Cat SCR019), anti-BLBP 1:500 (Chemicon Cat AB9558), anti-GFAP (Chemicon Cat SCR019), anti-betaIII tubulin 1:500 (Chemicon Cat SCR060), and anti-MAP2 1:200 (Chemicon SCR019). Secondary antibodies were Alexa Fluor 488 (goat anti-rabbit IgG, Invitrogen Cat A-11008) at 1:200 and Alexa Fluor 555 (goat anti-mouse IgG, Invitrogen Cat A-21422) at 1:200.

Normal human astrocytes (NHA) were obtained from Lonza and propagated according to the manufacturer's specifications.

FACS Analysis

CD133 (Miltenyi Biotec CD133/1 PE cat # 130-080-801 and SSEA-1 (BD Biosciences cat # 560127) antibodies were used according to manufacturer's instruction. For TF staining in primary tumor, primary human glioblastomas were obtained from patients operated at Massachusetts General Hospital in accordance with an approved IRB protocol (2005-P-001609/16). Briefly, tumors were dissociated to single cell suspension using a Brain Tumor Dissociation Kit (Miltenyi Biotec), depleted for CD45-positive immune cells using microbeads and a MACS separator (Miltenyi Biotec). Cells were stained with SOX2 (R+D Systems) and ASCL1 (BD Pharmingen) antibodies conjugated to Alexa Fluor 647 or Alexa Fluor 488 using Alexa Fluor Protein Labeling kits (Invitrogen). Flow cytometric analysis was conducted with an LSR II flow cytometer (BD Biosciences) and analysis was performed with FlowJo software (Treestar).

ChIP-Seq Assay

ChIP assays were carried out on cultures of approximately 1×10^6 cells per sample and epitope, following the general procedures outlined in (Ku et al., 2008; Mikkelsen et al., 2007). Immunoprecipitation was performed using antibodies against H3K4me3 (Millipore 07-473), H3K27me3 (Millipore 07449), H3K36me3 (Abcam 9050), H3K4me1 (Abcam 8895), ASCL1 (Epitomics T091) or LEF1 (Abcam 53293). ChIP DNA samples were used to prepare sequencing libraries, which were then sequenced on the Illumina Genome Analyzer II or HiSeq by standard procedures. We sequenced an input control for each cell type for use in normalization. Read alignment to the hg19 human reference genome was performed with Bowtie (Langmead et al., 2009) and density maps were generated with read extension to 200 bp with IGVtools (Robinson et al., 2011; Thorvaldsdottir et al., 2013). When several reads with same start position and direction were present, only one was kept for further analysis. Two replicates that were available for MGG8 GBM CSCs were merged into a single track. Visualization was performed with IGV. ChIP-Seq dataset statistics are summarized in **Table S1** and data are available for viewing at http://www.broadinstitute.org/cgi-bin/epigenomics/public/prod/cloneportal.cgi?data=rheinbay_GBMSC.

DNA methylation assay and analysis

For each sample, about 1×10^6 cells were harvested and genomic DNA was isolated using the QiaAMP DNA mini kit following manufacturer's instructions. DNA was eluted in 100 μL water, treated with RNase (37°C for 30 mins), cleaned up again with the QiaAMP DNA mini kit.

Data were processed using the Illumina BeadStudio software. Probes with p-value calls above 0.05 were discarded and values for two replicates for each sample were averaged. Probes with 0.75 were classified as "hypermethylated". Data are available through GEO (GSE46016).

Detection of regions enriched for histone modifications

Genomic regions enriched for a histone mark were identified using a sliding window approach as previously described (Mikkelsen et al., 2007) with several modifications. We adapted the previous approach for the highly copy-number variant genomes of the GBM CSCs with the help of an unenriched input sequencing track generated from whole-cell extract (WCE). In short, a fixed size window of 1 kb was used to scan the genome in 100 bp steps for local enrichment of ChIP signal. Significance of signal in each window was assessed based on the assumption that random read alignment would follow a Poisson distribution with parameter λ_{ChIP} . λ_{ChIP} was adjusted for local variation in genome copy number by multiplication with the observed-to-expected ratio (O/E) for unenriched input reads in this region (Mikkelsen et al., 2010). To increase numeric stability in regions of heterozygous deletions, we calculated this O/E ratio based on input reads in the scoring window as well as in a 10 kb and a 100 kb region centered at the current window, and used the maximal value of these three. When all three input O/E ratios were zero, $\lambda_{\text{adjusted}}$ was set to equal λ_{ChIP} . Poisson p-values were then calculated for each window with $\lambda_{\text{adjusted}}$. P-values were corrected for multiple-hypothesis testing using the Benjamini-Hochberg procedure (Benjamini and Hochberg, 1995) and only windows with significance $p < 10^{-5}$ were kept. Finally, adjacent (distance 1kb) enriched windows were merged into a single interval. For histone modifications in NS and NHA cells, we applied the same algorithm and parameters albeit without background correction. Genomic regions enriched for ASCL1 or LEF1 were identified with MACS (Zhang et al., 2008) No background correction as described above was applied; instead, peaks identified in the WCE track served to remove spurious TF peaks.

Transcription start sites (TSS) for genes from the hg19 human genome assembly were defined as region from 500 bp upstream to 2 kb downstream as previously described (Mikkelsen et al., 2007). Chromatin state calls for transcription start sites were then made based on a minimal overlap of 500 bp of enriched intervals with the 2.5 kb TSS region. A consensus set of TSS chromatin states in the CSCs was generated with the chromatin state of the majority (3 out of 4 CSC lines) assigned to summarized "CSC" cell type. 87% (n=20,422) of TSS satisfied the majority criterion and were thus included in the consensus set.

Functional gene enrichment analysis

Functional enrichment in gene sets was determined using the DAVID functional annotation tool with "FAT" GeneOntology terms (Dennis et al., 2003; version 6.7). Benjamini-Hochberg p-values correcting for multiple hypothesis testing were used for further interpretation.

Generation of aberrantly active TF set

TFs were identified as those aberrantly active genes that were contained in the GO:0003700 transcription factor activity set or in the set of human TFs defined in (Vaquerizas et al., 2009). We manually removed TFs whose chromatin state was incorrectly or ambiguously called by our algorithm to generate the final list of TFs. *MYCN* was also removed because of focal amplification in the MGG8 cell line. For the TF chromatin state heatmap, we extracted H3K4me3 and H3K27me3 signal, respectively, in 40 bins covering a 5 kb region around the annotated TSS from density maps. For both H3K4me3 and H3K27me3, several control genes with similar chromatin state in all samples were chosen (Table S4) and served to scale signal for each sample. TFs were ordered based on their H3K27me3 signal using hierarchical clustering (R, 2008), and H3K4me3 and H3K27me3 maps were overlayed to generate the final map. Cells exceeding 15% of maximum signal for H3K4me3 and H3K27me3 (“bivalent”) were additionally enhanced with orange color.

RNA extraction and gene expression analyses

Total RNA was isolated from cells using Trizol Reagent (Invitrogen) and purified using the RNeasy Kit (Qiagen). Gene expression data were acquired with Affymetrix Human Genome U133 2.0 Arrays. CEL files were normalized with RMA and multiple probe sets per gene were collapsed by taking the maximum expression value using the GenePattern package (Reich et al., 2006). Gene expression data for NHA was included from Balani et al., 2009. (GSE12305). Normal brain and astrocytoma transcriptome profiles were used from (Sun et al., 2006; GSE4290) and processed as described above. TCGA combined expression data and subtype information was obtained from (Verhaak et al., 2010).

Motif analyses

We used the HOMER software package (Heinz et al., 2010) to search for *de novo* enriched motifs in TF peak regions.

Overexpression and knockdown experiments

Human cDNA for *ASCL1*, *OLIG1*, *OLIG2*, *HEY2*, *LHX2* and *EN2* were cloned into a lentiviral plasmid and sequence verified. Primers used are listed in Table S6. For knockdown experiments, *ASCL1* lentiviral shRNA set from Open Biosystems was used (RHS4533-NM_004316) of which TRCN0000013551 (CCCGAACTGATGCCGTGCAAA) yielded sufficient knockdown. The same sequence was also used in vector pGIPZ (RHS4430-101103529) to allow for GFP sorting. Lentiviruses were produced as previously described (Barde et al., 2010). Briefly, cDNA coding or shRNA plasmids were cotransfected with *GAG/POL* and *VSV* plasmids into 293T packaging cells to produce the virus used to infect the target cells (NHA or GBM CSC). Viral supernatant was concentrated by ultracentrifugation using an SW41Ti rotor (Beckman Coulter) at 28,000 rpm for 120 min. Using GFP control, efficiency of infection was estimated as greater than 90% (data not shown). For maximal homogeneity, NHA were selected using 0.75 ug/ml puromycin for 5 days and GBM CSC were either selected using 2 ug/ml puromycin or sorted for GFP depending on vector used. After selection, RNA was extracted (Qiagen RNeasy kit) following manufacturer's instructions.

Real-time quantitative reverse transcriptase-PCR

For gene expression assays, cDNA was obtained using Moloney murine leukemia virus reverse transcriptase and RNase H minus (Promega). Typically, 250 ng of template total RNA and 250 ng of random hexamers were used per reaction. Real-time PCR amplification was performed using Power SYBR mix and specific PCR primers, in a 7500 Fast PCR instrument (Applied Biosystems). Relative quantification of each target, normalized to an

endogenous control (GAPDH), was performed using the comparative Ct method (Applied Biosystems). Error bars indicate standard error of the mean. Primer sequences are listed in **Table S6**.

Luciferase assay

TOPFLASH-Firefly and FOPFLASH-Renilla plasmids were co-transfected with *ASCL1* lentivirus or control vector in 293T cells using Fugene6, as previously described (Firestein et al., 2008; Veeman et al., 2003). When indicated, Wnt3a was added at 100ng/ml (R&D 5036-WN-010). Luciferase activity was measured after 48 hours using a Dual-Luciferase Reporter assay System (Promega E1910) according to manufacturer's instructions.

Sphere-formation assay

GFP-sorted GBM CSC spheres, infected either with lentiviral control vector or with *ASCL1* shRNA vector, were mechanically dissociated into single cells and plate at a density of one cell per well in 96 well plates, in triplicate. Sphere number was assessed 2 weeks later under a fluorescence microscope. For sphere diameter quantification, five pictures were taken per condition at 100x magnification. At least 60 spheres per conditions were measured with Image J.

Tumorigenicity study

Intracranial injections of 5000 cells from acutely dissociated gliomaspheres were performed with a stereotactic apparatus (Kopf Instruments) at coordinates 2.2 mm lateral relative to Bregma point and 2.5 mm deep from dura mater. Four severe combined immunodeficient (SCID) mice were used per condition. Kaplan-Meier curves and statistical significance (log-rank test) were calculated with the R survival package (R, 2008). Animal experiments were approved by protocol number 2009N000061.

RNA in-situ hybridization (ISH)

mRNA was detected in FFPE (formalin-fixed, paraffin-embedded) tissue sections using Quantigene ViewRNA (Affymetrix, CA). Probes for *ASCL1* (type 1, red, VA1-11908, Affymetrix, CA) and *Sox2* (type 6, blue, VA-11765) were used following the manufacturer's instructions for two-color chromogenic ISH. Tissue sections were prepared for hybridization by fixation in 10% formaldehyde, deparaffinization, boiling for 10 minutes, and digestion with protease for 20 minutes. Hybridization was performed for 2 hours at 40°C. Signal amplification and detection were performed using standard conditions for Fast Red and Fast Blue substrates. Tissues were counterstained with hematoxylin and visualized with a standard bright field microscope.

Supplementary Material

Refer to Web version on PubMed Central for supplementary material.

Acknowledgments

We thank Tarjei Mikkelsen, Timothy Durham and Noam Shores for computational assistance and Chuck Epstein, Robbyn Issner and the Broad Institute Genome Sequencing Platform for help with data production. We thank David Dombrowski for help with FACS analysis, and Lauren Solomon and Leslie Gaffney for assistance with graphics. A.S.C is supported by a Joan Ambriz American Brain Tumor Association Basic Research Fellowship and Early Career research award from the Ben and Catherine Ivy Foundation. M.L.S is supported by Oncosuisse grant BIL-KFS-02590-02-2010 and a Medic Foundation grant. M.N.R is supported by awards from the Burroughs Wellcome Fund and the Howard Hughes Medical Institute. S.D.R. supported in part by NIH (RO1 CA160762). This research was supported by funds from the Starr Cancer Consortium (B.E.B.), the Harvard Stem Cell Institute, the Burroughs

Wellcome Fund (B.E.B.) and the Howard Hughes Medical Institute (B.E.B.). M.N.R. and M.S. receive research funding from Affymetrix.

References

- Balani P, Boulaire J, Zhao Y, Zeng J, Lin J, Wang S. High mobility group box2 promoter-controlled suicide gene expression enables targeted glioblastoma treatment. *Mol Ther.* 2009; 17:1003–1011. [PubMed: 19240692]
- Bao S, Wu Q, McLendon RE, Hao Y, Shi Q, Hjelmeland AB, Dewhirst MW, Bigner DD, Rich JN. Glioma stem cells promote radioresistance by preferential activation of the DNA damage response. *Nature.* 2006; 444:756–760. [PubMed: 17051156]
- Barde I, Salmon P, Trono D. Production and titration of lentiviral vectors. *Curr Protoc Neurosci.* 2010 Chapter 4, Unit 4 21.
- Baylin SB, Jones PA. A decade of exploring the cancer epigenome - biological and translational implications. *Nat Rev Cancer.* 2011; 11:726–734. [PubMed: 21941284]
- Bell O, Tiwari VK, Thoma NH, Schubeler D. Determinants and dynamics of genome accessibility. *Nat Rev Genet.* 2011; 12:554–564. [PubMed: 21747402]
- Benjamini Y, Hochberg Y. Controlling the False Discovery Rate: A Practical and Powerful Approach to Multiple Testing. *Journal of the Royal Statistical Society Series B (Methodological).* 1995; 57:289–300.
- Birney E, Stamatoyannopoulos JA, Dutta A, Guigo R, Gingeras TR, Margulies EH, Weng Z, Snyder M, Dermitzakis ET, Thurman RE, et al. Identification and analysis of functional elements in 1% of the human genome by the ENCODE pilot project. *Nature.* 2007; 447:799–816. [PubMed: 17571346]
- Bruggeman SW, Hulsman D, Tanger E, Buckle T, Blom M, Zevenhoven J, van Tellingen O, van Lohuizen M. Bmi1 controls tumor development in an Ink4a/Arf-independent manner in a mouse model for glioma. *Cancer Cell.* 2007; 12:328–341. [PubMed: 17936558]
- Chen J, Li Y, Yu TS, McKay RM, Burns DK, Kernie SG, Parada LF. A restricted cell population propagates glioblastoma growth after chemotherapy. *Nature.* 2012; 488:522–526. [PubMed: 22854781]
- Clement V, Sanchez P, de Tribolet N, Radovanovic I, Ruiz i Altaba A. HEDGEHOG-GLI1 signaling regulates human glioma growth, cancer stem cell self-renewal, and tumorigenicity. *Curr Biol.* 2007; 17:165–172. [PubMed: 17196391]
- Clevers H. Wnt/beta-catenin signaling in development and disease. *Cell.* 2006; 127:469–480. [PubMed: 17081971]
- Conti L, Pollard SM, Gorba T, Reitano E, Toselli M, Biella G, Sun Y, Sanzone S, Ying QL, Cattaneo E, Smith A. Niche-independent symmetrical self-renewal of a mammalian tissue stem cell. *PLoS Biol.* 2005; 3:e283. [PubMed: 16086633]
- Dennis G Jr, Sherman BT, Hosack DA, Yang J, Gao W, Lane HC, Lempicki RA. DAVID: Database for Annotation, Visualization, and Integrated Discovery. *Genome Biol.* 2003; 4:P3. [PubMed: 12734009]
- ENCODE Project Consortium, E. P. Dunham I, Kundaje A, Aldred SF, Collins PJ, Davis CA, Doyle F, Epstein CB, Fretzke S, Harrow J, et al. An integrated encyclopedia of DNA elements in the human genome. *Nature.* 2012; 489:57–74. [PubMed: 22955616]
- Ernst J, Kheradpour P, Mikkelsen TS, Shores N, Ward LD, Epstein CB, Zhang X, Wang L, Issner R, Coyne M, et al. Mapping and analysis of chromatin state dynamics in nine human cell types. *Nature.* 2011
- Firestein R, Bass AJ, Kim SY, Dunn IF, Silver SJ, Guney I, Freed E, Ligon AH, Vena N, Ogino S, et al. CDK8 is a colorectal cancer oncogene that regulates beta-catenin activity. *Nature.* 2008; 455:547–551. [PubMed: 18794900]
- Galli R, Binda E, Orfanelli U, Cipelletti B, Gritti A, De Vitis S, Fiocco R, Foroni C, Dimeco F, Vescovi A. Isolation and characterization of tumorigenic, stem-like neural precursors from human glioblastoma. *Cancer Res.* 2004; 64:7011–7021. [PubMed: 15466194]

- Gangemi RM, Griffero F, Marubbi D, Perera M, Capra MC, Malatesta P, Ravetti GL, Zona GL, Daga A, Corte G. SOX2 silencing in glioblastoma tumor-initiating cells causes stop of proliferation and loss of tumorigenicity. *Stem Cells*. 2009; 27:40–48. [PubMed: 18948646]
- Heinz S, Benner C, Spann N, Bertolino E, Lin YC, Laslo P, Cheng JX, Murre C, Singh H, Glass CK. Simple combinations of lineage-determining transcription factors prime cis-regulatory elements required for macrophage and B cell identities. *Mol Cell*. 2010; 38:576–589. [PubMed: 20513432]
- Hulleman E, Quarto M, Vernell R, Masserdotti G, Colli E, Kros JM, Levi D, Gaetani P, Tunici P, Finocchiaro G, et al. A role for the transcription factor HEY1 in glioblastoma. *J Cell Mol Med*. 2009; 13:136–146. [PubMed: 18363832]
- Huse JT, Holland EC. Targeting brain cancer: advances in the molecular pathology of malignant glioma and medulloblastoma. *Nat Rev Cancer*. 2010; 10:319–331. [PubMed: 20414201]
- Joo KM, Kim SY, Jin X, Song SY, Kong DS, Lee JI, Jeon JW, Kim MH, Kang BG, Jung Y, et al. Clinical and biological implications of CD133-positive and CD133-negative cells in glioblastomas. *Lab Invest*. 2008; 88:808–815. [PubMed: 18560366]
- Ku M, Koche RP, Rheinbay E, Mendenhall EM, Endoh M, Mikkelsen TS, Presser A, Nusbaum C, Xie X, Chi AS, et al. Genomewide analysis of PRC1 and PRC2 occupancy identifies two classes of bivalent domains. *PLoS Genet*. 2008; 4:e1000242. [PubMed: 18974828]
- Langmead B, Trapnell C, Pop M, Salzberg SL. Ultrafast and memory-efficient alignment of short DNA sequences to the human genome. *Genome Biol*. 2009; 10:R25. [PubMed: 19261174]
- Lee J, Kotliarov S, Kotliarov Y, Li A, Su Q, Donin NM, Pastorino S, Purow BW, Christopher N, Zhang W, et al. Tumor stem cells derived from glioblastomas cultured in bFGF and EGF more closely mirror the phenotype and genotype of primary tumors than do serum-cultured cell lines. *Cancer Cell*. 2006; 9:391–403. [PubMed: 16697959]
- Lee J, Son MJ, Woolard K, Donin NM, Li A, Cheng CH, Kotliarov S, Kotliarov Y, Walling J, Ahn S, et al. Epigenetic-mediated dysfunction of the bone morphogenetic protein pathway inhibits differentiation of glioblastoma-initiating cells. *Cancer Cell*. 2008; 13:69–80. [PubMed: 18167341]
- Ligon KL, Alberta JA, Kho AT, Weiss J, Kwaan MR, Nutt CL, Louis DN, Stiles CD, Rowitch DH. The oligodendroglial lineage marker OLIG2 is universally expressed in diffuse gliomas. *J Neuropathol Exp Neurol*. 2004; 63:499–509. [PubMed: 15198128]
- Lottaz C, Beier D, Meyer K, Kumar P, Hermann A, Schwarz J, Junker M, Oefner PJ, Bogdahn U, Wischhusen J, et al. Transcriptional profiles of CD133+ and CD133-glioblastoma-derived cancer stem cell lines suggest different cells of origin. *Cancer Res*. 2010; 70:2030–2040. [PubMed: 20145155]
- Meissner A, Mikkelsen TS, Gu H, Wernig M, Hanna J, Sivachenko A, Zhang X, Bernstein BE, Nusbaum C, Jaffe DB, et al. Genome-scale DNA methylation maps of pluripotent and differentiated cells. *Nature*. 2008; 454:766–770. [PubMed: 18600261]
- Mikkelsen TS, Ku M, Jaffe DB, Issac B, Lieberman E, Giannoukos G, Alvarez P, Brockman W, Kim TK, Koche RP, et al. Genome-wide maps of chromatin state in pluripotent and lineage-committed cells. *Nature*. 2007; 448:553–560. [PubMed: 17603471]
- Murat A, Migliavacca E, Gorlia T, Lambiv WL, Shay T, Hamou MF, de Tribolet N, Regli L, Wick W, Kouwenhoven MC, et al. Stem cell-related “self-renewal” signature and high epidermal growth factor receptor expression associated with resistance to concomitant chemoradiotherapy in glioblastoma. *J Clin Oncol*. 2008; 26:3015–3024. [PubMed: 18565887]
- Ohm JE, McGarvey KM, Yu X, Cheng L, Schuebel KE, Cope L, Mohammad HP, Chen W, Daniel VC, Yu W, et al. A stem cell-like chromatin pattern may predispose tumor suppressor genes to DNA hypermethylation and heritable silencing. *Nat Genet*. 2007; 39:237–242. [PubMed: 17211412]
- Osada H, Tomida S, Yatabe Y, Tatematsu Y, Takeuchi T, Murakami H, Kondo Y, Sekido Y, Takahashi T. Roles of achaete-scute homologue 1 in DKK1 and E-cadherin repression and neuroendocrine differentiation in lung cancer. *Cancer Res*. 2008; 68:1647–1655. [PubMed: 18339843]
- Parsons DW, Jones S, Zhang X, Lin JC, Leary RJ, Angenendt P, Mankoo P, Carter H, Siu IM, Gallia GL, et al. An integrated genomic analysis of human glioblastoma multiforme. *Science*. 2008; 321:1807–1812. [PubMed: 18772396]

- Pujadas E, Feinberg AP. Regulated noise in the epigenetic landscape of development and disease. *Cell*. 2012; 148:1123–1131. [PubMed: 22424224]
- R, DCT. A Language and Environment for Statistical Computing.. Vienna Austria R Foundation for Statistical Computing 1. 2008.
- Reich M, Liefeld T, Gould J, Lerner J, Tamayo P, Mesirov JP. GenePattern 2.0. *Nat Genet*. 2006; 38:500–501. [PubMed: 16642009]
- Robinson JT, Thorvaldsdottir H, Winckler W, Guttman M, Lander ES, Getz G, Mesirov JP. Integrative genomics viewer. *Nat Biotechnol*. 2011; 29:24–26. [PubMed: 21221095]
- Schlesinger Y, Straussman R, Keshet I, Farkash S, Hecht M, Zimmerman J, Eden E, Yakhini Z, Ben-Shushan E, Reubinoff BE, et al. Polycomb-mediated methylation on Lys27 of histone H3 pre-marks genes for de novo methylation in cancer. *Nat Genet*. 2007; 39:232–236. [PubMed: 17200670]
- Schwartzentruber J, Korshunov A, Liu XY, Jones DT, Pfaff E, Jacob K, Sturm D, Fontebasso AM, Quang DA, Tonjes M, et al. Driver mutations in histone H3.3 and chromatin remodelling genes in paediatric glioblastoma. *Nature*. 2012; 482:226–231. [PubMed: 22286061]
- Shih AH, Holland EC. Notch signaling enhances nestin expression in gliomas. *Neoplasia*. 2006; 8:1072–1082. [PubMed: 17217625]
- Singh SK, Clarke ID, Terasaki M, Bonn VE, Hawkins C, Squire J, Dirks PB. Identification of a cancer stem cell in human brain tumors. *Cancer Res*. 2003; 63:5821–5828. [PubMed: 14522905]
- Singh SK, Hawkins C, Clarke ID, Squire JA, Bayani J, Hide T, Henkelman RM, Cusimano MD, Dirks PB. Identification of human brain tumour initiating cells. *Nature*. 2004; 432:396–401. [PubMed: 15549107]
- Son MJ, Woolard K, Nam DH, Lee J, Fine HA. SSEA-1 is an enrichment marker for tumor-initiating cells in human glioblastoma. *Cell Stem Cell*. 2009; 4:440–452. [PubMed: 19427293]
- Stricker SH, Feber A, Engstrom PG, Caren H, Kurian KM, Takashima Y, Watts C, Way M, Dirks P, Bertone P, et al. Widespread resetting of DNA methylation in glioblastoma-initiating cells suppresses malignant cellular behavior in a lineage-dependent manner. *Genes Dev*. 2013; 27:654–669. [PubMed: 23512659]
- Sun L, Hui AM, Su Q, Vortmeyer A, Kotliarov Y, Pastorino S, Passaniti A, Menon J, Walling J, Bailey R, et al. Neuronal and glioma-derived stem cell factor induces angiogenesis within the brain. *Cancer Cell*. 2006; 9:287–300. [PubMed: 16616334]
- Suva ML, Riggi N, Janiszewska M, Radovanovic I, Provero P, Stehle JC, Baumer K, Le Bitoux MA, Marino D, Cironi L, et al. EZH2 is essential for glioblastoma cancer stem cell maintenance. *Cancer Res*. 2009; 69:9211–9218. [PubMed: 19934320]
- Thorvaldsdottir H, Robinson JT, Mesirov JP. Integrative Genomics Viewer (IGV): high-performance genomics data visualization and exploration. *Brief Bioinform*. 2013; 14:178–192. [PubMed: 22517427]
- Travis A, Amsterdam A, Belanger C, Grosschedl R. LEF-1, a gene encoding a lymphoid-specific protein with an HMG domain, regulates T-cell receptor alpha enhancer function [corrected]. *Genes Dev*. 1991; 5:880–894. [PubMed: 1827423]
- Valent P, Bonnet D, De Maria R, Lapidot T, Copland M, Melo JV, Chomienne C, Ishikawa F, Schuringa JJ, Stassi G, et al. Cancer stem cell definitions and terminology: the devil is in the details. *Nat Rev Cancer*. 2012; 12:767–775. [PubMed: 23051844]
- Vaquerizas JM, Kummerfeld SK, Teichmann SA, Luscombe NM. A census of human transcription factors: function, expression and evolution. *Nat Rev Genet*. 2009; 10:252–263. [PubMed: 19274049]
- Veeman MT, Slusarski DC, Kaykas A, Louie SH, Moon RT. Zebrafish prickle, a modulator of noncanonical Wnt/Fz signaling, regulates gastrulation movements. *Curr Biol*. 2003; 13:680–685. [PubMed: 12699626]
- Verhaak RG, Hoadley KA, Purdom E, Wang V, Qi Y, Wilkerson MD, Miller CR, Ding L, Golub T, Mesirov JP, et al. Integrated genomic analysis identifies clinically relevant subtypes of glioblastoma characterized by abnormalities in PDGFRA, IDH1, EGFR, and NF1. *Cancer Cell*. 2010; 17:98–110. [PubMed: 20129251]

- Wakimoto H, Kesari S, Farrell CJ, Curry WT Jr, Zaupa C, Aghi M, Kuroda T, Stemmer-Rachamimov A, Shah K, Liu TC, et al. Human glioblastoma-derived cancer stem cells: establishment of invasive glioma models and treatment with oncolytic herpes simplex virus vectors. *Cancer Res.* 2009; 69:3472–3481. [PubMed: 19351838]
- Wakimoto H, Mohapatra G, Kanai R, Curry WT Jr, Yip S, Nitta M, Patel AP, Barnard ZR, Stemmer-Rachamimov AO, Louis DN, et al. Maintenance of primary tumor phenotype and genotype in glioblastoma stem cells. *Neuro Oncol.* 2011
- Widschwendter M, Fiegl H, Egle D, Mueller-Holzner E, Spizzo G, Marth C, Weisenberger DJ, Campan M, Young J, Jacobs I, Laird PW. Epigenetic stem cell signature in cancer. *Nat Genet.* 2007; 39:157–158. [PubMed: 17200673]
- Wu G, Broniscer A, McEachron TA, Lu C, Paugh BS, Becksfort J, Qu C, Ding L, Huether R, Parker M, et al. Somatic histone H3 alterations in pediatric diffuse intrinsic pontine gliomas and non-brainstem glioblastomas. *Nat Genet.* 2012
- Zhang N, Wei P, Gong A, Chiu WT, Lee HT, Colman H, Huang H, Xue J, Liu M, Wang Y, et al. FoxM1 Promotes beta-Catenin Nuclear Localization and Controls Wnt Target-Gene Expression and Glioma Tumorigenesis. *Cancer Cell.* 2011; 20:427–442. [PubMed: 22014570]
- Zhang Y, Liu T, Meyer CA, Eeckhoute J, Johnson DS, Bernstein BE, Nussbaum C, Myers RM, Brown M, Li W, Liu XS. Model-based analysis of ChIP-Seq (MACS). *Genome Biol.* 2008; 9:R137. [PubMed: 18798982]
- Zheng H, Ying H, Wiedemeyer R, Yan H, Quayle SN, Ivanova EV, Paik JH, Zhang H, Xiao Y, Perry SR, et al. PLAGL2 regulates Wnt signaling to impede differentiation in neural stem cells and gliomas. *Cancer Cell.* 2010; 17:497–509. [PubMed: 20478531]
- Zhou VW, Goren A, Bernstein BE. Charting histone modifications and the functional organization of mammalian genomes. *Nat Rev Genet.* 2011; 12:7–18. [PubMed: 21116306]
- Zhu J, Adli M, Zou JY, Verstappen G, Coyne M, Zhang X, Durham T, Miri M, Deshpande V, De Jager PL, et al. Genome-wide Chromatin State Transitions Associated with Developmental and Environmental Cues. *Cell.* 2013; 152:642–654. [PubMed: 23333102]

Highlights

- Epigenomic profiles of glioblastoma stem cells and comparators
- An aberrant network of developmental transcription factors in cancer stem cells
- ASCL1 is essential for glioblastoma stem cell maintenance and tumorigenicity
- ASCL1 activates Wnt signaling by directly repressing the negative regulator DKK1

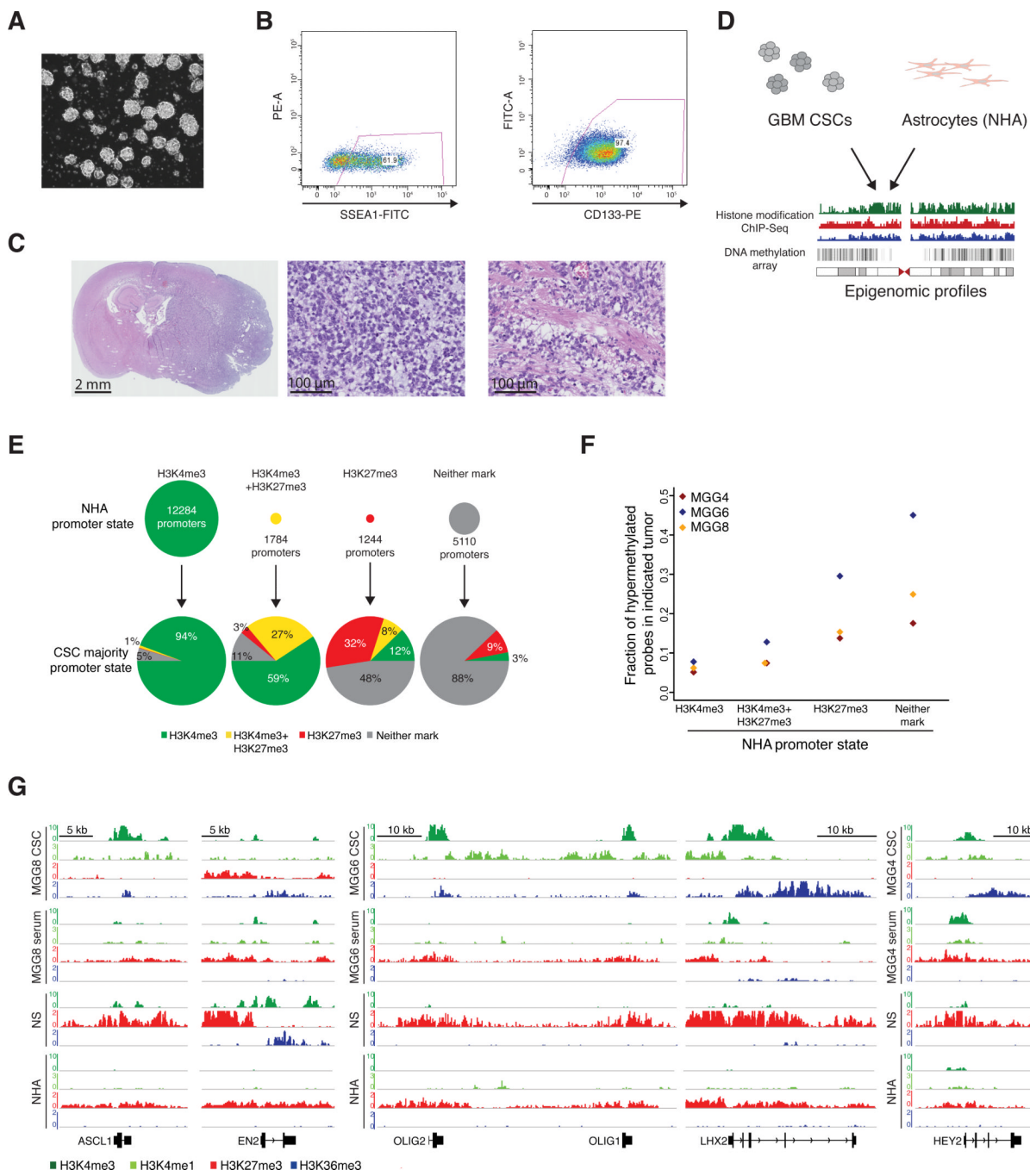
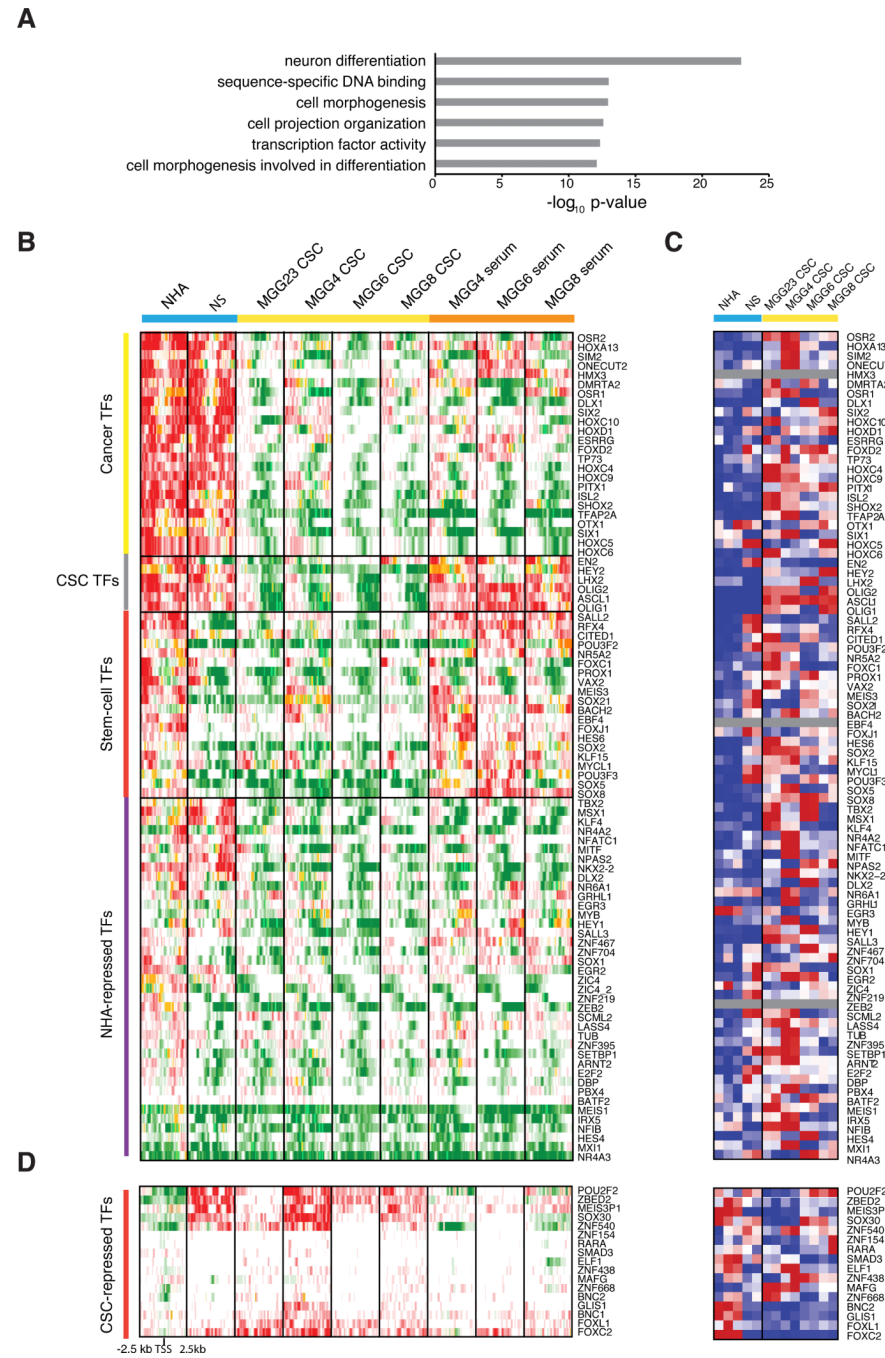


Figure 1. Characterization of the GBM CSC chromatin landscape

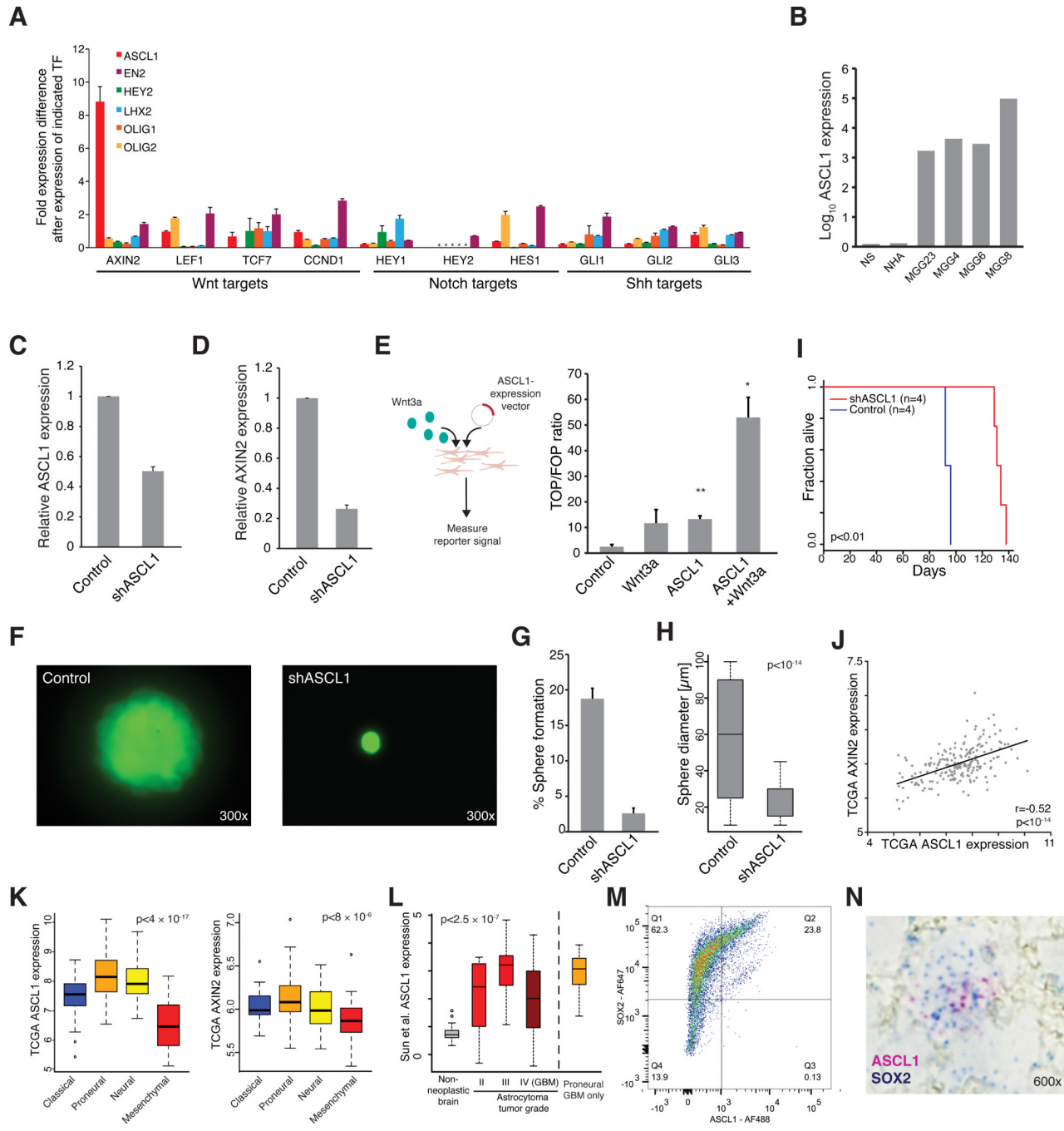
(A) GBM CSCs used for this study grow as gliomaspheres in serum-free neurobasal media. (B) FACS analysis of MGG8 GBM CSCs shows positivity for the GBM stem cell markers SSEA-1 and CD133. (C) Mouse brain cross-section after orthotopic xenotransplantation of MGG8 GBM CSCs (left). Higher magnification of tumor tissue depicts cytonuclear pleomorphism, mitotic and apoptotic figures (center) and infiltration along white matter tracks (right). (D) Schematic overview of study strategy. (E) Breakdown of TSS chromatin state in NHA (H3K4me3 only, H3K4me3+H3K27me3, H3K27me3 only, neither mark) and their consensus chromatin state in the GBM CSCs (see Experimental Procedures). A large fraction (59%) of genes bivalent in NHA becomes activated (H3K4me3 only, green) in

GBM CSCs. (F) Fraction of DNA hyper-methylated (> 0.75) probes in MGG4, MGG6, and MGG8 GBM CSCs contingent on NHA chromatin state of the probe. Probes marked with H3K27me3 only are twice as likely to become DNA methylated than those marked with both H3K4me3 and H3K27me3. (G) Chromatin state of six CSC-TFs in one representative GBM CSC line, matched serum-grown GBM cell line, NS and NHA. All TFs are active (H3K4me3 at promoter, H3K36me3 over the transcript) in GBM CSCs, but not NHA or serum-grown GBM cells as indicated by large domains of H3K27me3.

**Figure 2. Aberrant activation and repression of TF Polycomb targets in GBM CSCs**

(A) Representative top scoring functional terms enriched in genes active (H3K4me3 only) in GBM CSCs but repressed in NHA (see also **Table S3**). Scores are calculated based on Benjamini-Hochberg corrected p-values (see Experimental procedures). (B) H3K4me3 (green) and H3K27me3 signal (red) at aberrantly activated TF loci (-2.5kb to +2.5 kb from TSS) for indicated cell types. Orange indicates overlap of H3K4me3 and H3K27me3 signal (“bivalent”). Genes were clustered based on H3K27me3 signal. (C) Microarray gene expression data for activated TFs confirms chromatin state data (GSE46016). Red indicates high, blue low expression normalized by row. The expression changes are consistent with the chromatin changes, although the magnitude of expression change across samples is more

variable. (D) Chromatin state and gene expression data for NHA-active, GBM CSC repressed TF loci. Color scheme as in (B) and (C).

**Figure 3. ASCL1 is an upstream regulator of the Wnt pathway**

(A) Relative expression of Wnt, Notch and Shh targets after ectopic lentiviral expression of indicated TF in NHA measured by RT-qPCR. * indicates not detectable. (B) mRNA levels of *ASCL1* in NS, NHA and GBM CSCs measured on Affymetrix microarray (GSE46016). (C) Relative levels of *ASCL1* after shRNA-mediated knock-down MGG4 CSCs by RT-qPCR. (D) Repression of *AXIN2* upon knockdown of *ASCL1* in MGG4 CSCs (t-test p<0.005). (E) Schematic of Wnt activation experiment and relative luciferase expression for a TCF/LEF-responsive promoter (TOPFLASH-Firefly) relative to a scrambled response element (FOPFLASH-Renilla) in 293T cells after lentiviral transfection with *ASCL1* and addition of Wnt3a. ** indicates one-tailed t-test p<0.01, * indicates p<0.05. Individual

examples (F) and quantification (G) of MGG4 CSC sphere-forming capacity in control and *ASCL1*-depleted cells. (H) Quantification of sphere diameter in control and *ASCL1*-depleted cells. (I) Kaplan-Meier survival curve for mice injected with 5,000 control (blue line) or *ASCL1*-depleted MGG4 CSCs (log-rank p-value <0.01). (J) Scatter plot shows correlation between *AXIN2* and *ASCL1* expression across 200 primary GBM samples (Verhaak et al., 2010). Each point denotes a single tumor sample. (K) TCGA *ASCL1* (left) and *AXIN2* (right) expression (Verhaak et al., 2010) correlate across molecular subtypes. Distributions for subtypes are significantly different from each other (Kruskal-Wallis $p<4 \times 10^{-17}$ (*ASCL1*) and $p<8 \times 10^{-6}$ (*AXIN2*)). (L) *ASCL1* expression (Sun et al., 2006) is increased in GBM, most strongly in the proneural subtype, and lower grade astrocytomas, relative to non-neoplastic brain, suggesting that *ASCL1* induction may be an early event in gliomagenesis. (M) Intracellular staining and flow cytometric detection of the nuclear stem cell marker SOX2 and ASCL1 in primary GBM. The population of ASCL1+ cells (23.8%) is entirely contained within the SOX2+ compartment. Notably, the ASCL1+ subpopulation also displays highest levels of SOX2 expression. (N) RNA-ISH for *SOX2* (blue dots) and *ASCL1* (red dots) in primary GBM shows expression of *ASCL1* in a restricted subset of *SOX2*+ cells.

Error bars in RT-qPCR experiments indicate standard error of the mean.

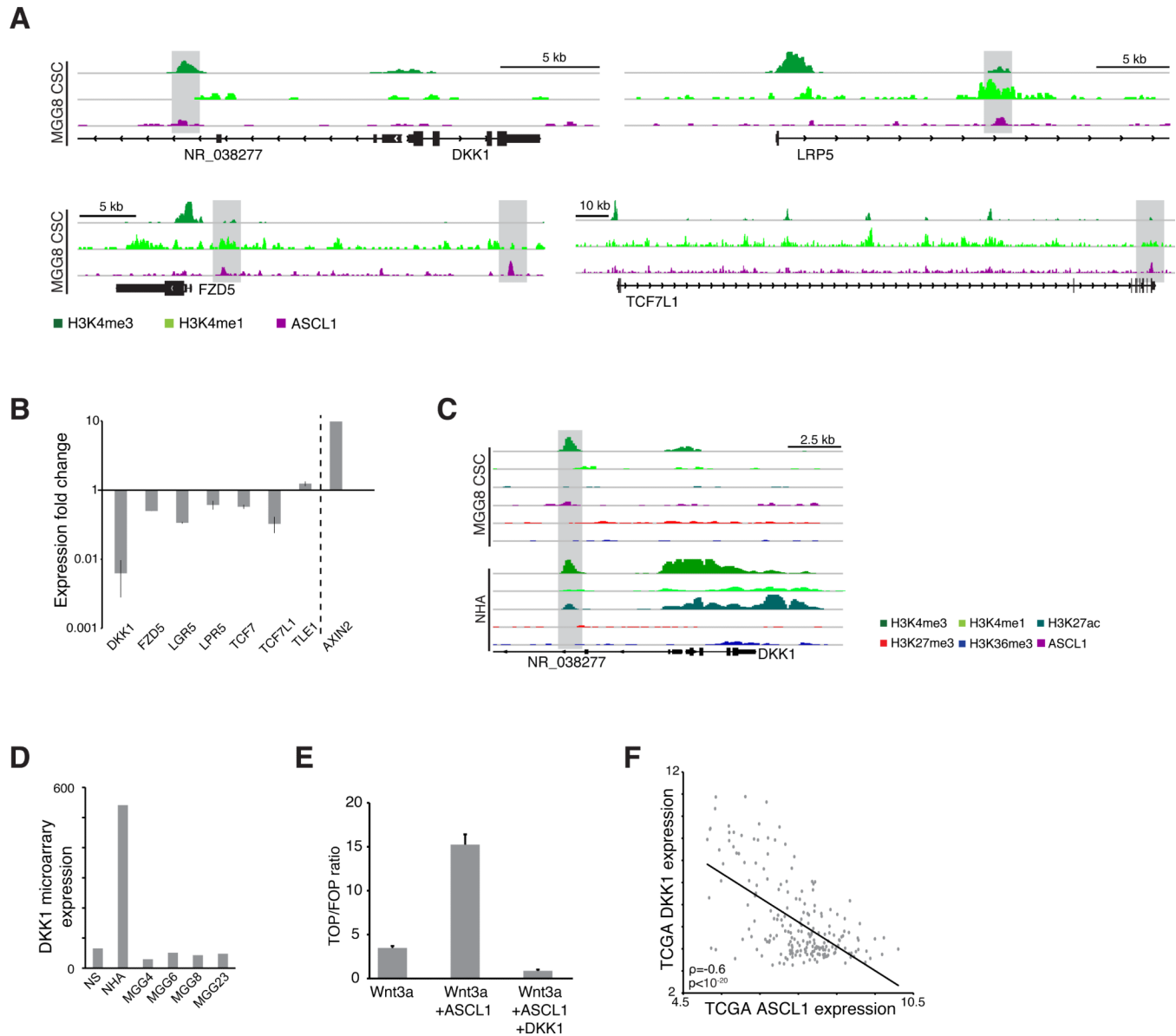


Figure 4. ASCL1 regulates Wnt signaling through DKK1

(A) ChIP-Seq of ASCL1 in MGG8 CSCs (pink track) reveals enrichment at H3K4me1-marked distal elements in several Wnt pathway gene loci (grey shading). (B) Relative mRNA level change for ASCL1-bound Wnt pathway genes in NHA after ectopic expression of ASCL1. (C) ChIP-Seq maps depict the chromatin environment of the *DKK1* gene locus and the ASCL1-bound enhancer (grey shading) in MGG8 CSCs and NHA. In the absence of ASCL1, the element is activated (as indicated by H3K27 acetylation in NHA) and *DKK1* is expressed (increase in active marks H3K4me3, H3K4me1, H3K27ac and H3K36me3). (D) Expression levels of *DKK1* in NS, NHA and GBM CSCs measured by microarray. (E) Expression changes of a TCF/LEF-responsive reporter (TOPFLASH-Firefly) relative to scrambled response elements (FOPFLASH-Renilla) in 293T cells after stimulation with the indicated combinations of Wnt3a protein and lentivirally-transfected *ASCL1* and *DKK1*. *DKK1* overexpression abrogates ASCL1-mediated Wnt induction. (F) *DKK1* and *ASCL1* expression patterns are inversely correlated in 200 GBM samples (Verhaak et al., 2010). Each point denotes a tumor sample.

Error bars in RT-qPCR experiments indicate standard error of the mean.

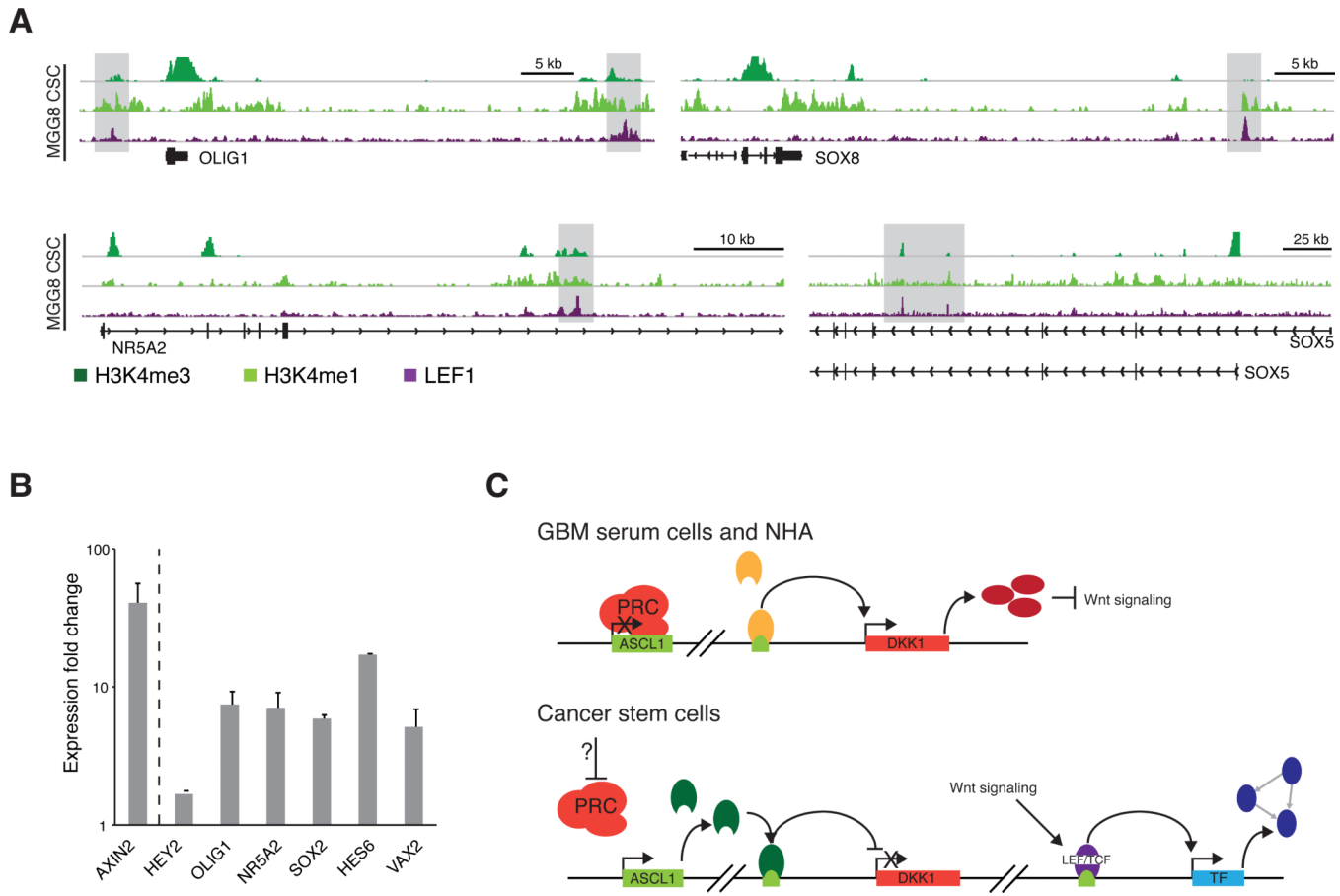


Figure 5. Cross-talk of the TF module and Wnt signaling in GBM CSCs

(A) ChIP-Seq of LEF1 (purple track) in MGG8 CSCs reveals enrichment at H3K4me1-marked distal elements near several TF loci. (B) Relative mRNA level changes for Wnt-responsive TFs with distal elements bound by LEF1 after transfection of NHA with ASCL1 and stimulation with Wnt3a measured by RT-qPCR. Error bars indicate standard error of the mean.

(C) A model for cross-talk between aberrantly activated TFs and Wnt signaling in non-stem GBM cells and NHA (top) versus GBM CSCs (bottom). In non-stem GBM cells and NHA, Polycomb complexes repress TFs, including *ASCL1*. In the absence of *ASCL1* protein, the *DKK1* upstream regulatory elements is active, the locus is transcribed, and expressed *DKK1* inhibits Wnt signaling. In GBM CSCs, Polycomb repression is lost at many TF loci, including *ASCL1*. *ASCL1* binds to the *DKK1* regulatory element, thereby repressing *DKK1* expression and activating Wnt signaling. Active Wnt signaling feeds back upon loci encoding several other TFs that are aberrantly active in GBM CSCs.